

Electrochemical Corrosion Behaviour of Different Cu-Base Alloys in Concentrated LiBr Solutions: Part II- Brass (Cu/30 Zn) Alloy

A. E. El Melleigy¹, A. A. El Warraky¹, Sh. E. Abd El hamid¹, El-Sayed M. Sherif^{1,2,*}

¹ Electrochemistry and Corrosion Laboratory, Department of Physical Chemistry, National Research Centre, El-Behoth St. 33, Dokki, Cairo 12622, Egypt.

² Center of Excellence for Research in Engineering Materials (CEREM), King Saud University, P.O. Box 800, Al-Riyadh 11421, Saudi Arabia.

*E-mail: esherif@ksu.edu.sa ; emsherif@gmail.com

Received: 8 October 2019 / Accepted: 13 January 2020 / Published: 10 February 2020

The corrosion behaviour of brass (Cu/30Zn) alloy in 4M LiBr solution was investigated by the cyclic potentiodynamic polarization and current-time measurements. The work was complemented by the use of scanning electron microscopy (SEM) and the energy dispersive X-ray (EDX) analysis techniques. Cyclic potentiodynamic polarization indicated that the current of the Cu/30Zn alloy increases linearly and a plateau area was appearing with increasing the applied potential. The oxide film formed on the surface of the alloy was not passive or protective and the dissolution of Cu/30Zn alloy occurred via general corrosion. The pitting attack was not recognized as there was no hysteresis loop observed at all conditions. The results obtained from the SEM micrographs and EDX profile analyses confirmed that the ratio of Cu to Zn on the surface was found higher than that detected from matrix of the alloy. The mechanism of corrosion of the Cu/30Zn alloy via the dezincification of the surface was found to occur by a simultaneous dissolution.

Keywords: brass alloy; chronoamperometry; corrosion; dezincification; surface analysis

1. INTRODUCTION

Absorption technology is one of the best choice to compression cooling in terms of energy diversification and environmental protection [1]. Recently, the triple effect absorption cycle has attracted much interest to replace the conventional machine as the more efficient one [2]. The absorption system such as absorption chillers and heat transformer is very attractive in the aspect of energy consumption and environmental problem and the demand of these machines is on an increasing trend [3].

Copper and copper alloys are commonly used in the manufacture of absorption machines and heat exchangers pipes due to high thermal conductivity. Different Cu-alloys containing one of metals

like Fe, Zn, Ni, Co, Al, and Sn, which are commonly used, the so-called Cu-binary alloys. The most common dissolution of these binary alloys occurs as a consequence of dealloying phenomena [4].

Dealloying is an electrochemical reaction in which the less noble metal constituent of the alloy is preferentially removed leaving surface rich in the more noble metal. The most susceptible alloys are the ones containing metals with high distance between each other in the galvanic series e.g. copper and zinc in brass (dezincification) and copper-nickel (denickelification) [5-10]. Two main theories have been put forward to explain the dezincification mechanism of brass. One of them proposes the selective dissolution of Zn from the alloy leaving a porous residue rich in metallic Cu, while the other proposes the simultaneous dissolution of both Zn and Cu after that the subsequent stage Cu redeposit from solution at sites close to where the brass was dissolved [11-16]. The mechanism of the dezincification was dependent on the potential of the alloy. When the potentials lie between -0.9 - 0.0 V [17-19], the mechanism is one of preferential dissolution of zinc, the rate of dezincification is slow. Where as in the range 0.0-0.2 V, the alloy dissolves with copper redeposition, the rate of dezincification is higher, while at potentials above 0.2 V, both zinc and copper dissolve without redeposition of copper.

The conventional LiBr/H₂O solution is the most commonly employed refrigerant absorbent couple in absorption systems due to its favorable thermophysical properties. However, LiBr can cause a serious corrosion problem to the metal part of the machine operating. In aqueous environments [20,21] the corrosion of metals takes places through electrolyte transport from the bulk solution to the metal surface then electrode exchange at the electrode/ solution interface leading to metal loss and transport of corrosion product from the interface to the bulk solution. Several authors [22-27] have studied the corrosion of different Cu-alloys in LiBr solutions in different conditions. This study aims to explore the effect of corrosion product films of brass (Cu/30Zn) in concentrated LiBr solution using electrochemical measurement and surface analysis techniques. Also the study is extended to explain the dezincification mechanism.

2. EXPERIMENTAL PROCEDURES

The preparation of the samples, the chemicals, materials, and the electrochemical measurements along with the surface pre-treatment and surface analysis techniques have been reported in our previous work [28]. In brief, an electrochemical cell with three electrodes; a saturated calomel, platinum foil, and the brass alloy were respectively used as the reference, counter and the working electrodes. All electrochemical experiments were collected by the use of a PS6 Meinsberger Potentiostat/ Galvanostat.

The cyclic potentiodynamic polarization experiments were recorded in various molar concentrations of the LiBr solutions. Prior the polarization measurements, the potential of the brass alloy was stepped to -600 mV (SCE) for 20 min in the LiBr solution. The polarization data were obtained via scanning the potential of the brass alloy in the range from -600 mV in the more positive direction and to +800 mV at a scanning rate of 1 mV/s. The scan was performed again in the backward direction at the same scan rate to close the circle and to better report the pitting corrosion.

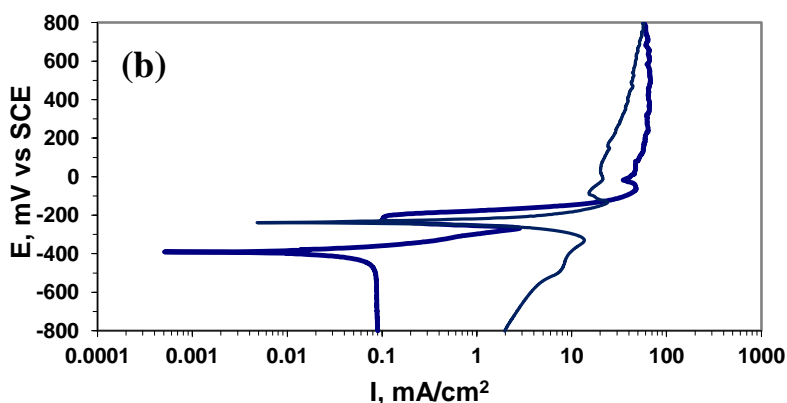
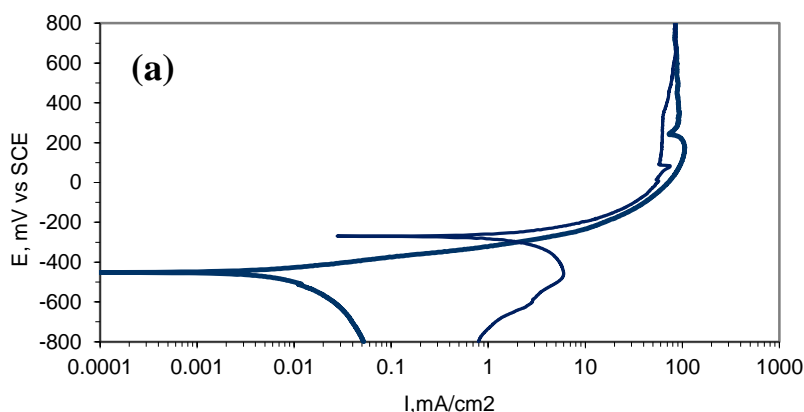
The change of current versus time experiments were performed via applying a value of a constant voltage, which was -200 mV (SCE) for 2.0 hours. A set from the test alloys were collected to be surface analyzed. Here, these samples were perfectly cleaned for 0.5 hour in bidistilled water using ultrasonic

vibration before being dried between fibreless tissues and were quickly placed inside the vacuum chamber of a scanning electron microscope (JXA-840A electron probe microanalyzer (SEM), JEOL). This SEM machine was also equipped with an energy dispersive X-ray (EDX, JXA-840A) electron probe microanalyzer, which was also made by JEOL. A Perkin-Elmer type 2380 atomic absorption spectrophotometer was employed to perform the analysis of the solution after carrying out the corrosion tests.

3. RESULTS AND DISCUSSION

3.1. Cyclic potentiodynamic polarization

The effect of different concentration of LiBr on the dissolution of Cu/30Zn was investigated. Figure 1(a) show the cyclic anodic polarization of Cu/30Zn in 4M LiBr which was taken as a blank and is called the first cycle. It can be seen from Figure 1(a) that the corrosion potential (E_{Corr}) recorded at -455 mV and the maximum current (I_{max}) was recorded at 104 mA. At such concentration, the anodic reaction is essentially limited by the applied potential where the bromide ions have little significant effect as shown in following equation



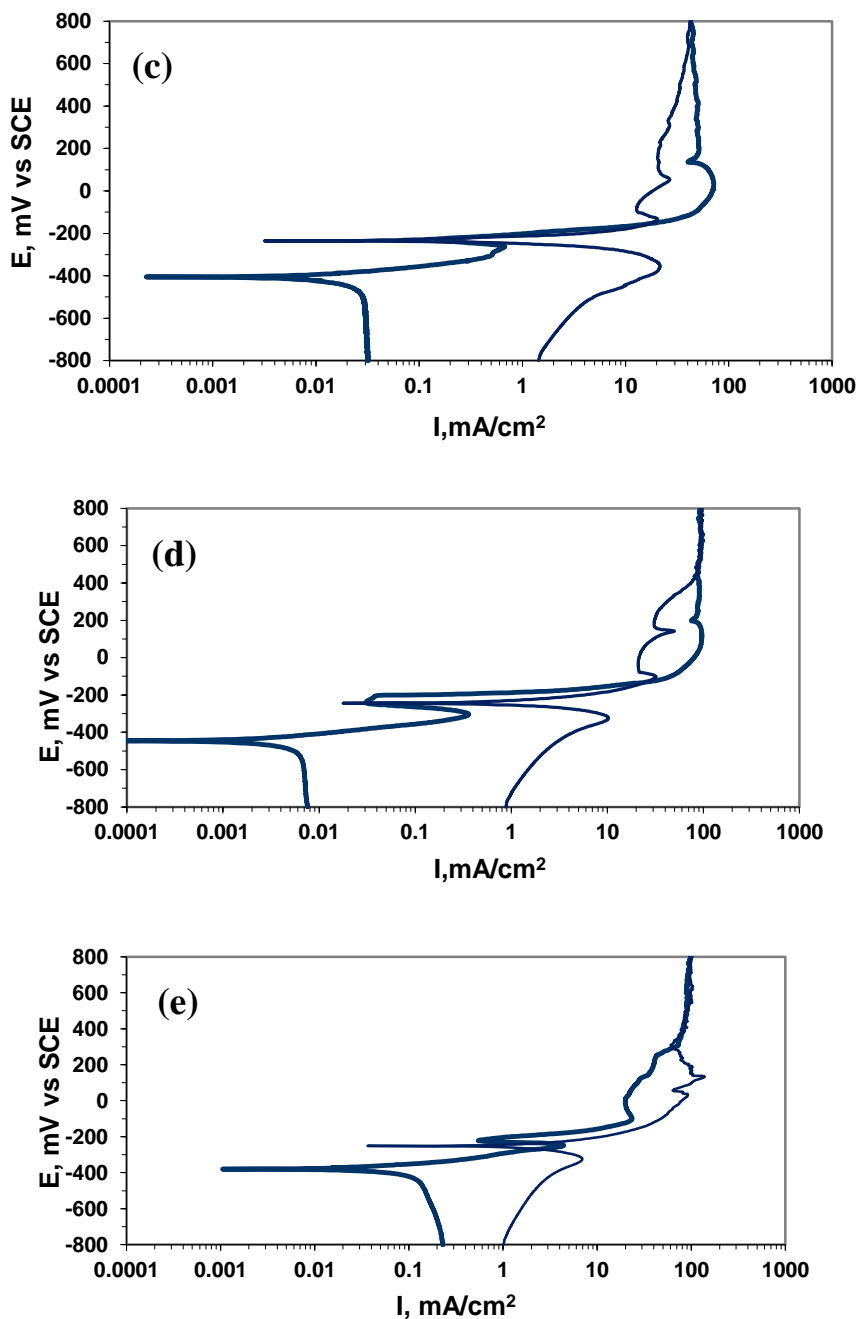


Figure 1. Potentiodynamic polarization for Cu/30 Zn in 4 M LiBr solution, (a) without SCP and with SCP of each of (b) Cu/30Zn alloy, (c) Cu/10Ni alloy, (d) Cu/30Ni alloy, and (e) Cu/7Al alloy, respectively. The bold line represents the forward potential scanning direction, while the narrow line represents the backward scanning direction.

Figure1 (a) represents that, the dissolution current is occur under charge transfer control where the current increases linearly with potential. After that a plateau of current was appearing with increasing the potential, which represent that the dissolution reaction is controlled by mass transport of CuBr_2^- through CuBr formed film as follows [29];



Or the occurrence of autocatalytic reaction as [30-32];



As shown by Eq. (5), Cu^{2+} is the dominant soluble species at higher potential. This is in agreement with the Pourbaix diagram for Cu/H₂O [33], which shows that this higher dissolution is consistent with the formation of Cu^{2+} soluble species. This behavior of the brass alloy is very similar to that observed previously [34-36] and concluded that the predominant species in the film formed at higher concentrations of NaCl or LiBr was mainly CuCl or CuBr depending on the anion used.

To clarify the effect of corrosion product on the surface and in the solution, a new sample of Cu/30Zn was treated in the resulted solution of the first cycle, which containing soluble corrosion product (SCP) of different Cu alloys, namely Cu/10Ni, Cu/30Ni and Al-bronze. The second cyclic was performed in the resulted solution but with a new sample, i.e. new sample of Cu/30Zn in solution of soluble corrosion product of the first cyclic of Cu/30Zn. By the same manner, the second cycle of Cu/30Zn alloy in the resulted solution of the first cycle of each of Cu/10Ni, Cu/30Ni and Cu/7Al alloys is shown in Figure 1 (b-e) respectively. All the curves of Figure 1(b-e) and Table 1 show that the corrosion potential have a singularity negative value in comparison with that of the blank (the first cyclic). On the other hand, the curve of Figure 1(b-e) recorded that the appearance of one peak after the active dissolution region where its maximum, I_{max} , is between 40 mA and 90 mA depending on the alloy used and the dissolution of the Cu/30Zn alloy occurs by general dissolution.

Table 1. Corrosion parameters for Cu/30 Zn in solution of Cu/10Ni, Cu/30 Zn, Cu/7 Al, and Cu/30Ni in 4M LiBr solution.

Corrosion products	$E_{\text{Corr}}/$ mV	$E_{\text{P}}/$ mV	$I_{\text{P}}/$ μA	$E_{\text{Pit}}/$ mV	$I_{\text{Pit}}/$ μA	$E_{\text{RP}}/$ mV	$I_{\text{RP}}/$ μA	$E_{\text{Pit}}-E_{\text{RP}}/$ mV	$I_{\text{max}}/$ μA
Cu/30Zn in 4M LiBr (blank)	-460	-265	-340	0.04	—	—	—	—	—
In solution Cu/10Ni	-390	-250	-270	3	-135	0.05	-220	0.12	85
In solution Cu/30Zn	-370	-240	-250	4.55	-130	0.04	-240	0.08	110
In solution Cu/7Al	-375	-240	-265	1.98	-235	0.06	-240	0.3	5
In solution Cu/30Ni	-380	-200	-260	2.6	-140	0.06	-200	0.08	60

Here, E_{pit} is the pitting potential, I_{pit} is the pitting current, E_{Corr} is the corrosion potential, I_{Max} is the maximum current, E_{P} is the peak potential, I_{P} is the peak current, E_{rp} is representing the repassivation potential, I_{rp} is the repassivation current, and $E_{\text{Pit}} - E_{\text{rp}}$ is the area of the hysteresis loop.

It is seen that the Cu/30Zn alloy in the second cycle in solution of SCP of Cu/7Al recorded an appearance of a hysteresis loop area in a partial passive region at higher potential and not in the passive region. This indicates that pitting corrosion occurs as a result of the accumulation of the corrosion product on the surface of the alloy.

3.2. Current – time measurement

In order to shed more light on the corrosion behavior of the brass alloy in the different LiBr solutions and whether pitting corrosion takes place at a constant active anodic value of value of potential, the current-time measurements were carried out. Figure 2 shows the variation in the current density with time that was collected for Cu/30 Zn alloy in (a) 4M LiBr, (b) 6M LiBr, and (c) 9M LiBr solutions, respectively at a constant potential of -200 mV (SCE). The curves of Figure 2 show a general feature where, a sudden decrease in the initial current densities at the first moment of polarization and after that, steady states in current were attained at 2.63, 5.8, 16.23 mA/cm² for 4M, 6M, 9M LiBr solutions, respectively. Also, the increase in the current density at the steady state was occurring as a result of the competitive between the dissolution and the oxide film formation and a partially current is produced. Moreover, the obtained current-time curves confirmed that there is a similarity in the behavior for all concentrations of LiBr test solutions and there is no any oscillations or fluctuations recorded on the curves. This is in a good agreement with the cyclic potentiodynamic polarization data, which shows also the absence of any hysteresis loop area and indicated that only general dissolution can occur at this potential.

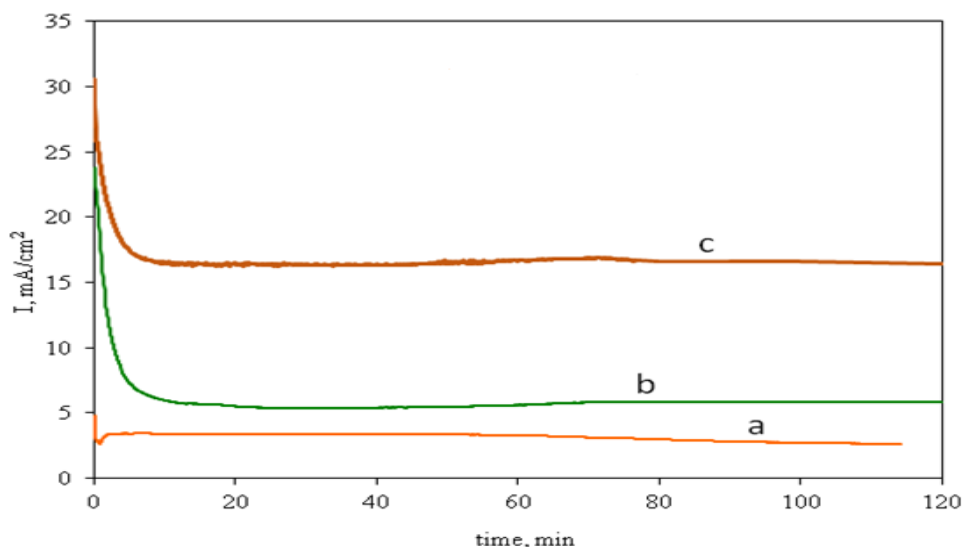


Figure 2. Current time curves collected for Cu/30Zn alloy in (a) 4M LiBr, (b) 6M LiBr, and (c) 9M LiBr solutions, respectively at a constant potential of -200 mV (SCE).

3.3. surface analysis examination

Examination of the formed film on the surface of Cu/30Zn alloy via SEM after being treated in 4M LiBr solution at a fixed potential value of -200 mV (SCE) for 120 min is shown in Figure 3. The micrograph of Figure 3(a) shows a very small amount of black spots. Increasing the magnification as seen from image (b) of Figure 3 confirmed the presence of these black spots. To clarify the presence of these findings, EDX profile analyses were performed on the surface of the Cu/30Zn alloy after being immersed in 4M LiBr solution and received an amount of -200 mV (SCE) for 120 min; i.e., at the end of experiment of Figure 2. The EDX elemental analysis spectra taken for the majority of the surface of Cu/30Zn alloy outside the black spot seen on Figure 3(b) are depicted by Figure 4. It is worth to mention

also that the EDX profile analysis was also collected inside the black spot shown by Figure 3(b) and the spectra for these elemental analysis are represented in Figure 5.

Several features have been understood from the EDX profiles shown in Figure 4 and Figure 5. First, the atomic conc. % (at. %) for both Cu and Zn outside the black spots is higher than that recorded inside the black spots. This occurs because a massive carbon was detected inside the spots and its at. % was 76.00%, while it was only 23.49% outside these spots. At this condition, the formation of Cu₂O or ZnO inside spots are dislike to take place and most probably is prevented. Moreover, the detection of this type of carbon was previously detected due to the presence of some defective points on the surface of the brass alloy, which are characterized by a shallow depression or cavities [34-38]. These depression or cavities are filled with some sorts of carbon species. The authors [34-38] suggested that the source of this carbon may be due to the adsorption of atmospheric hydrocarbon. A second feature is the detection of oxygen with higher concentration inside black spots than its outside, where it recorded 15.26 at. % and 7.15 at. %, respectively. This result is in good agreement with the previous studies [6-9] in which the investigators have concluded that the cavities (black spots) represent a rout by which the oxygen of the solution stays in contact with the interface of the alloys metal oxide to maintain the potential of the system at the potential of the metal/metal oxide. A third feature is the detection of Br with higher ratio outside the black spots than its inside, 0.61 at. % and 0.07 at. %, respectively. These confirm that each black spot represents a cavity or depression and does not consider as pitting corrosion form. The fourth and the last feature is the ratio of both Cu and Zn outside and inside spots are higher than its ratio in the alloy substrate as listed in Table 2 and indicate on the occurrence of the dezincification for the Cu/30Zn alloy at this condition. Also, the presence of O with higher ratio than Br for the outside of the black spots confirms that the surface was covered by Cu₂O and ZnO. This result is coinciding with the generally accept results which recorded previously [10,39]. These result reported that at the initial stages copper atoms cannot oxidized in the presence of Zn atoms. This is attributed to the solid state displacement reaction as follows;



Table 2. Solution analysis after different polarization times for Cu/30Zn in 4M LiBr solution.

Polarization time	Cu/30 Zn Alloy			
	Cu		Zn	
	ppm	%	ppm	%
After 5 min	0.40	40.0	0.60	60.0
After 30 min	1.30	76.4	0.40	28.5
After 60min	3.20	75.4	1.04	24.5
After 90 min	6.84	81.0	1.60	18.9
After 120 min	12.6	80.5	3.04	19.4

On the other hand, solution analysis of Table 2 reveals that, the presence of Cu and Zn from the beginning of polarization and their amount slightly increased by time. Table 2 shows that ratio of Cu/Zn in solution was smaller than that of the alloy substrate at all polarization time except at 5 min. where, its ratio is higher than the Cu/Zn ratio in the bulk alloy. This is support the simultaneous dissolution theory of Cu/Zn alloy. The ratio of Cu/Zn in solution is lower of Zn compared to the alloy bulk composition. This indicates that the growth of film formed on the surface and the dissolution of the alloy which is controlled by diffusion [10,39] depending on the ionic radii of Cu^+ and Zn^{2+} . Another information was obtained by a quantitative test of Cu analysis in solution using dimethyldithiocarbamate reagent, which detected that copper in solution is present mainly in the monovalent state (CuBr_2^-) and mentoring as Cu^{++} (CuBr_2). This reagent gives faint yellowish brown color with traces amount of Cu^{++} that changes to yellowish brown suspension with the increase of Cu^{++} content. The detection of divalent copper in solution is a strong support to the previously suggested autocatalytic reaction seen via Eq. (5). The amount of produced Cu^{++} ions seems to be enough to diffuse through the surface film and to go to the solution in spite of its accessibility to precipitation as metallic copper through a galvanic reaction with Zn as in this equation;

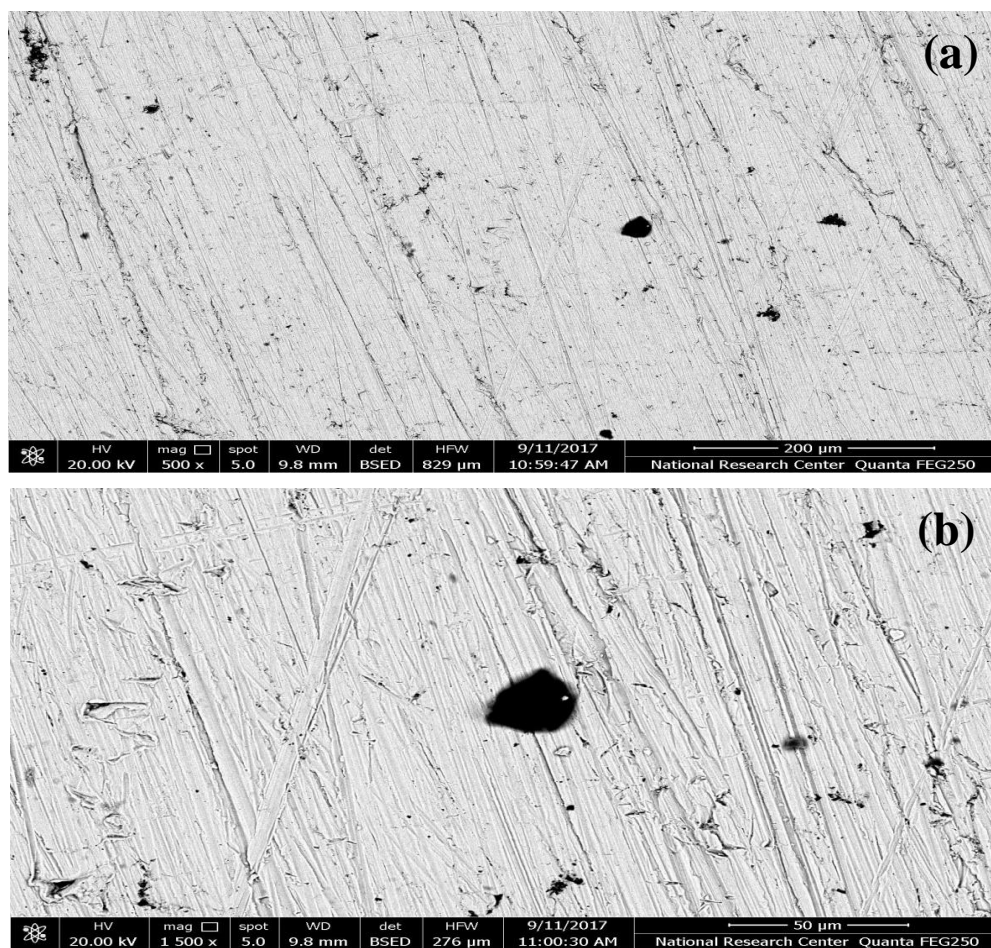


Figure 3. SEM micrographs obtained for Cu/30 Zn alloy in 4 M LiBr after stepping the potential to -200 mV (SCE) for 120 min.

These results were confirmed with the trend found by Saber and El warraky [7], when they polarized α -brass although, the trends are nearly the same, yet the absolute values are not the same because of difference in the corroding media in both cases. The corroding media were in 4% NaCl solution. Pickering and Byrne [40,41] reported that the decrease in the initial current as a result of the depletion of the alloy surface from the less noble constituent. They support the theory of selective dissolution mechanism. This depletion as they stated in a fall in the supply of the less noble metal to the alloy front and therefore its direct contact with the electrolyte was restricted. In the present work the drop in the current density recorded at the initial stages of current-time measurement can be explained as found by Saber and El warraky [7]. They used more advanced techniques such as XPS and AES and reported that the decrease in the current can reassembly be related to the changes that take place on the outer most layer of the Cu/30Zn surface after polarized in 4% NaCl. These changes arise from the formation of Cu₂O and ZnO which precipitated through the first few atomic layers during the early stages of polarization. This precipitated forms a barrier layer, which can restrict the electrolytic contact with the alloy surface.

The electrochemical dissolution of zinc occurs via one of the following reactions;



$$E = -0.76 + 0.0295 \log a \text{Zn}^{++},$$



$$K_{\text{sp}} = 8.41 \times 10^{-18} - 1.66 \times 10^{-16}$$



$$E = -0.439 - 0.0591 \text{pH}$$

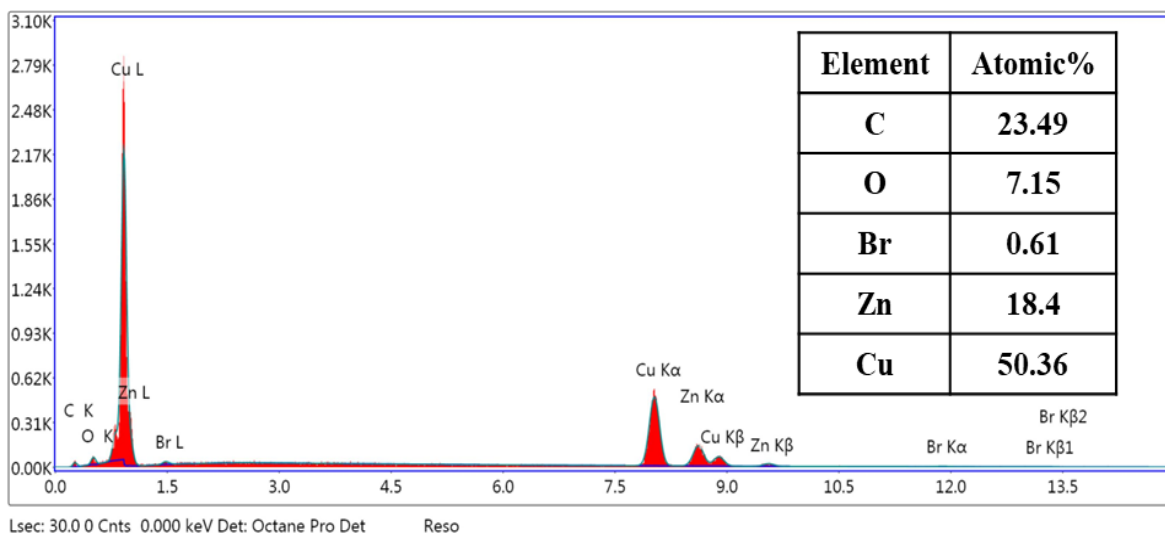


Figure 4. EDX profile analysis obtained outside the cavity of the SEM image shown in Figure 3b for the surface of the Cu/30Zn alloy in 4M LiBr after applying a potential value of -200 mV (SCE) for 120 min.

The presence of OH⁻ in Eq. (9) and Eq. (11) has resulted from the hydrolysis of water as per the following reaction;



On the other hand, the formation of the cuprous oxide (Cu₂O) might take place through Eq. (1), E = 0.52 + 0.0591 log a_{Cu⁺}, or Eq. (2), K_{sp} = 3.2x10⁻⁷, or Eq. (4), E_o = 0.62, or finally via the hydrolysis of the cuprous cations as per the following reaction, Eq. (13);

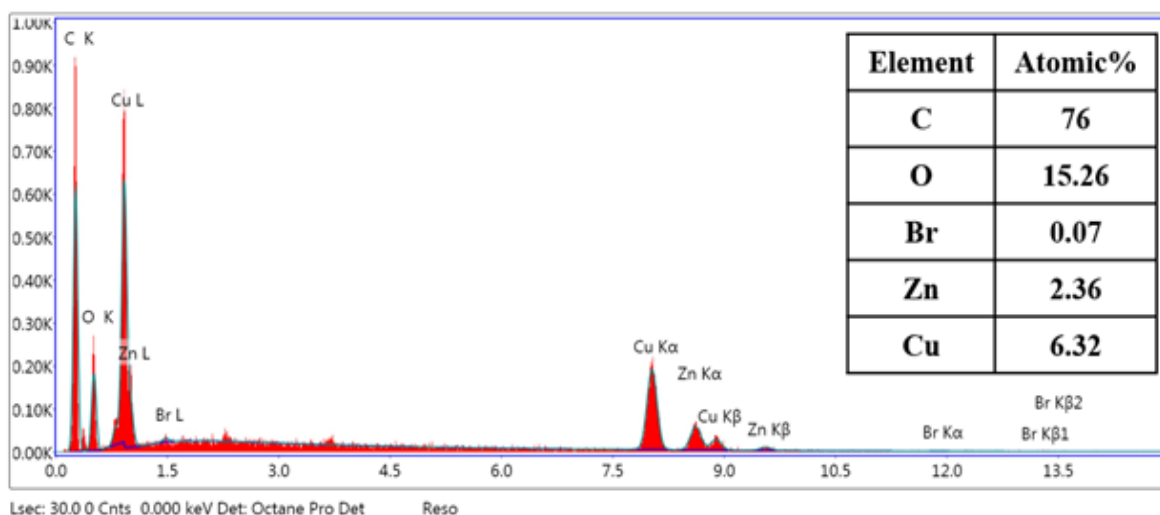
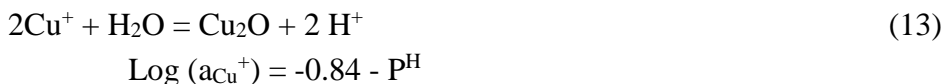


Figure 5. EDX profile analysis obtained inside the cavity of the SEM image shown in Figure 3b for the surface of the Cu/30Zn alloy in 4M LiBr after applying a potential value of -200 mV (SCE) for 120 min.

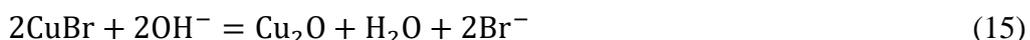
In view of the ambient pH (~ 9) of precipitation of Cu₂O as in Eq. (13), it will be dependent on how much Cu⁺ is produced. The produced amount of Cu⁺ is expected to be sufficient to precipitate Cu₂O on the surface and to go to the solution as confirmed previously in surface analysis using EDX and solution analysis by atomic absorption techniques. At a potential of -200 of Cu/30Zn in 4M LiBr, it is expected that the surface of the alloy undergoes relatively excessive electrochemical dissolution, where the rest potential is less noble than -200 mV, as shown by Eq. (1) and where the pH of the solution is slightly alkaline (~ 9), specially at the brass surface for Zn and Eq. (2) and Eq. (4) for Cu. Moreover, the surface of the alloy is covered by ZnO and Cu₂O only as revealed from the EDX analysis of Figure 5. Furthermore, CuBr is detected with very small amount on the alloy surface because it goes to the solution via Eq. (4) and /or hydrolysis to result in the formation of Cu₂O according to Eq. (3).

This is in agreement with the proposal of Saber and El warraky [7] on the filmed surface of Cu/30Zn in 4% NaCl. The authors justified the dissolution of the alloy at -250 mV through the accumulation of ZnO, which undergoes dissolution as bizincate ion (HZnO₂⁻) and Cu when ionized (Cu⁺) has a chance to go to solution as CuBr₂⁻ and to precipitate as Cu₂O. The authors [7] also found that after polarization of Cu/30Zn in 4% NaCl, Cu is detected on the surface mainly as CuCl, while Cu₂O and

metallic copper exist at lower level. Also, two zinc species of ZnO and HZnO_2^- are marginally and the peak of Zn metal is minor. These authors [7] attributed the detection of metallic copper and zinc to the thin nature of the formed film on the alloy surface and a higher Cu/Zn ratio on the surface, which shows a smaller ratio in the solution than in the alloy. These findings are not in agreement with the present results, which revealed that Cu and Zn are presented on the surface mainly as Cu_2O and ZnO and are associated with a trace amount of Br. On the other hand, the Cu/Zn ratio on the surface of Table 2 represents a higher value than that of the alloy matrix which means that the dezincification of the surface. Solution analysis represents that, after 5 min. of polarization the ratio of Cu/Zn is lower of Zn compared to alloy bulk composition. This occurs as a result of the film thickness formed on the alloy is small enough to make the alloy metallic character within the detection limit of EDX technique. The most important finding in the experimental result of EDX analysis is the detection of carbon on the alloy surface which effect on the fact value of the ratio of Cu/Zn. The at. % of carbon represented over 30% of the atom present. The source of carbon is the adsorption from the atmospheric hydrocarbon, where -200 mV is within the active dissolution of the alloy to make the surface becomes active enough to absorb carbon and oxygen from atmosphere. The real value of Cu and Zn on the surface is higher than the detected value because its thickness on the surface is very small in comparison with the escape depth of the EDX beam. This occurs as a result of the formation of the oxide films on the alloy's surface.

From these studies, we can conclude that the general dissolution of Cu/30Zn takes place through the porous Cu_2O film, which is not protective in 4M LiBr. Here, the mechanism of the dissolution of Cu/30Zn in 4M LiBr can be proposed in Figure 6 and as per the following steps;

The first step (a) is the formation of CuBr as shown by Eq. (2). The second step (b) becomes possible as the CuBr species may undergo hydrolysis as in Eq. (3) or due to the presence of hydroxide ion, where a porous Cu_2O is formed on the surface due to the cathodic reaction of oxygen reduction as follows;



At the same time of the formation of Cu_2O , there are small areas which are filled with a trapped CuBr underneath the formed Cu_2O and also the appearance of a massive carbon in the cavities or depressions as shown in step (c). Although the concentration of 4M LiBr solution is high, it can not cause pitting corrosion because the formed Cu_2O is not protective, where the hole produced due to the dissolution of Cu as CuBr_2^- cannot be filled by Zn. Accordingly, Br^- cannot attack the weak point of cavities through the trapped CuBr and only the general dissolution takes place. As increasing the concentration of CuBr_2^- soluble complex in LiBr solution, the bromide can undergo a disassociation reaction as follows;



Where, Cu can redeposit from solution as in step (d) or can act in the formation of Cu_2O as can be seen from Eq. (4). Also, the CuBr_2^- acts in the formation of the outer layer of Cu_2O through hydrolysis according to the reaction number (15). From all these steps of Figure 6, it can be said that the dissolution of the Cu/30Zn brass alloy passes through a simultaneous dissolution mechanism and only the general corrosion takes place.

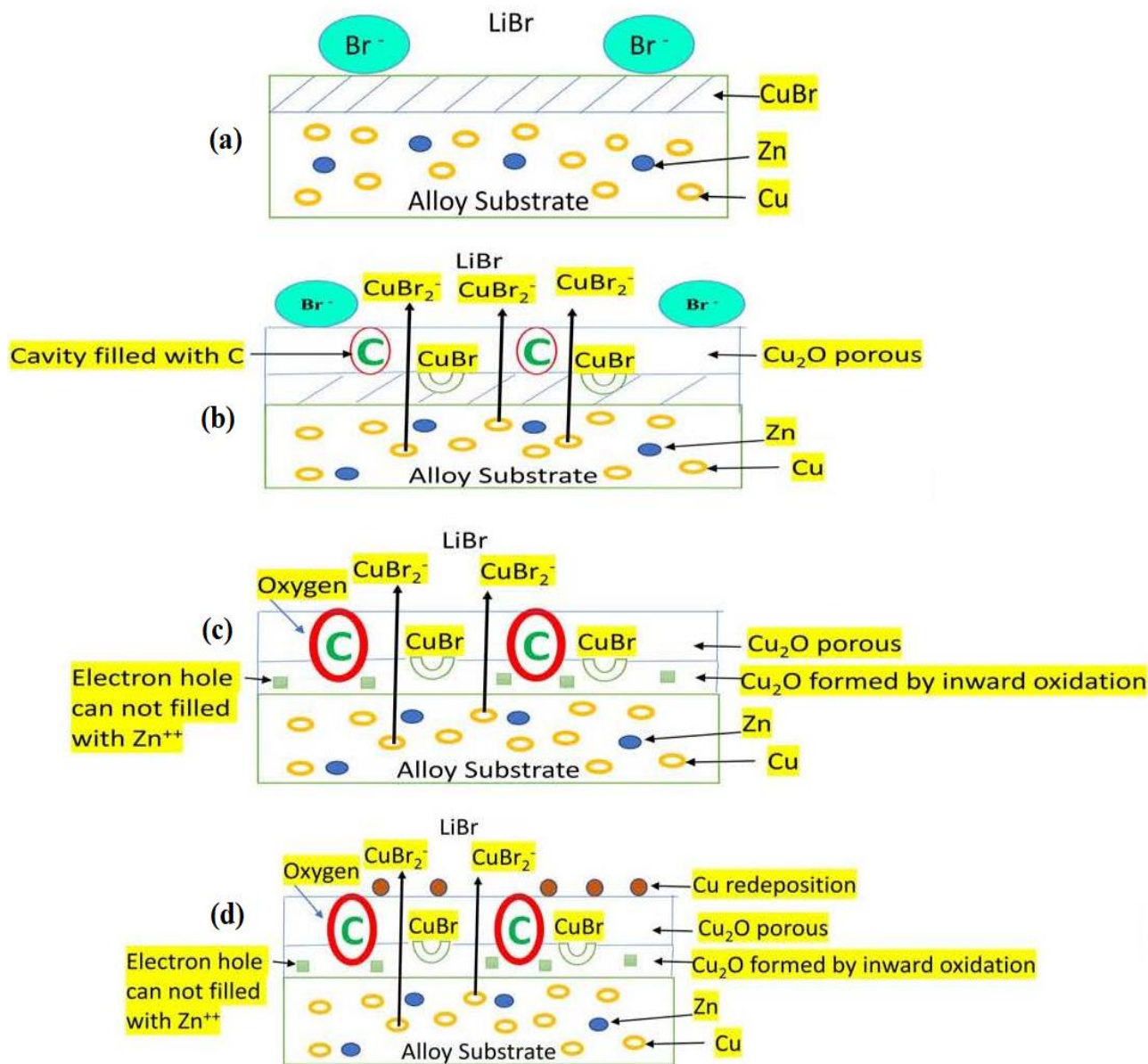


Figure 6. Schematic representation of the mechanism of the dissolution of Cu/30Zn alloy in heavy brine LiBr solutions.

4. CONCLUSIONS

The first cyclic polarization curve (blank) of Cu/30Zn in 4M LiBr was investigated. It can be seen that the dissolution reaction is controlled by mass transport of CuBr₂⁻ through film formed. The effect of SCP on the surface can be explained from the second cycle of Cu/30Zn in the resulted solution of the first cycle of each of Cu/10Ni, Cu/30Ni and Al-bronze revealed that the absence of hysteresis loop area and satisfy the general dissolution. Current –time measurements confirm the result of potentiodynamic polarization. The film formed on Cu/30Zn alloy after treated in 4M LiBr solution at -200 mV shows a very small amount of black spots. Br is higher outside than inside spots so that the black is cavity and not pitting. The result of surface examination EDX and solution analysis indicates

that the dissolution of the alloy is occurring by simultaneous dissolution mechanism. Cu and Zn % is higher outside cavities than inside and present on the surface as Cu₂O and ZnO, which associated with a trace amount of Br. The ratio of both Cu and Zn outside and inside cavities indicated the dezincification of the Cu/30Zn alloy.

ACKNOWLEDGMENT

Researchers Supporting Project number (RSP-2019/33), King Saud University, Riyadh, Saudi Arabia.

References

1. M.J. Munoz-Portero, J. Garcia-Anton, J.L. Guinon, V. Perez-Herranz, *Passivation of Metals and Semiconductors and Properties of Thin Oxide Layers*, 131 (2006).
2. J.S. Kim, Lee H. Fziegler, *Appl. Therm. Eng.*, 22 (2002) 295.
3. Young Park, Jin. Soo Kim, Huen Lee, *Int. J. Refrig.*, 20(5) (1997) 319.
4. A.E. Meleigy, A.M.A. Aziz, M.F. Shehata, Sh.E. Abd El Hamid, A.A. Warraky, *Egypt. J. Chem. Special Issue*, (2009) 93-110.
5. H.H. Uhlig, *Corrosion and Corrosion Control*, John Wiley, NY (1971).
6. T.M.H. Saber and A.A. El Warraky, *Brit. Corros. J.*, 26 (1991) 279.
7. T.M.H. Saber and A.A. El Warraky, *Desalination*, 93 (1993) 473.
8. T.M.H. Saber and A.A. El Warraky, *16th Annual Conf. Corrosion Problems in Industry*, Hurghada, Egypt 11 (1997) 29.
9. T.M.H. Saber and A.A. El Warraky, *17th Annual Conf. Corrosion Problems in Industry*, Zafarana, Egypt 1 (1998) 19.
10. A.A. El Warraky, *Brit. Corros. J.*, 32 (1997) 57.
11. R. Cerrato, A. Casal, M.P. Mateo, G. Nicolas, *Spectrochim. Acta part 3*, 130 (2017) 1.
12. A.A. El Warraky, A.E. El Meleigy, M.F. Shehata, *Mater. Sci., An Indian Journal*, 4(4) (2008) 248.
13. J. Mathiyarasy, N. Palaniswamy, V. S. Mualidaran, *Ind. J. Chem. Technol.*, 9 (2002) 350.
14. R.M. Horton, *Corrosion*, 26 (1970) 160.
15. H. Sugawara, E. Ebiko, *Corros. Sci.*, 7 (1967) 513.
16. H.W. Pickering, *J. Electrochem. Soc.*, 8 (1979) 117.
17. Seungman Sohn, Tak kang, *J. Alloys Compounds*, 335 (2002) 281.
18. R.H. Heidersbach, E.D. Verink, *Corrosion NACE*, 28 (1972) 397.
19. J.-Y. Zou, D.-H. Wang, W.-C. Qiu, *Electrochim. Acta*, 42 (1997) 1733.
20. K. Tanno, M. Itoh, T. Takahashi, H. Yashiro, N. Kumagai, *Corros. Sci.*, 34 (1993) 1441.
21. J.J. W. Furlong, *The Air Pollution Consultant* (11/12/1994) 1.12.
22. E. Sarmiento, J.G. Gonzalez-Rodriguez, J. Uruchurtu, O. Sarmiento, M. Menchaca, *Inter. J. Electrochem. Sci.*, 4 (2009) 144.
23. D.M. Garcia-Garcia, E. Blasco- Tanarit, J. Garcia-Anton, *Int. J. Electrochem. Sci.*, 6 (2011) 1237.
24. R.M. Fernandez- Domene, E. Blasco-Tamarit, D. M. Garcia-Garcia, J. Garcia-Anton, *Int. J. Electrochem. Sci.*, 6 (2011) 3292.
25. R. Leiva-Garcia, J. Garcia-Anton, M.J. Munoz-Portero, *Corros. Sci.*, 52 (2010) 950.
26. R. Leiva-Garcia, J. Garcia-Anton, M.J. Munoz-Portero, *Corros. Sci.*, 52 (2010) 2133.
27. E. Blasco- Tanarit, A. Igual-Munoz, J. Garcia-Anton, D. Garcia-Garcia, *Corros. Sci.*, 50 (2008) 1848.
28. A.E. El Meligy, Sh.E. Abd El Hamid, A.A. Elwarraky, *Mater. Sci. Eng. Technol. (Mater. Wiss. & Werkstofftech.)*, 46 (1) (2015); doi.org/10.1002/mawe.201400316.
29. A. Valero-Gomez, J. Garcia-Anton, A. Igual-Munoz, *Corrosion*, 62 (2006) 751.

30. A.A. El Warraky, A.E. El Meleigy, Sh.E. Abd El Hamid, *Egypt. J. Chem.*, 59 (2016) 833.
31. R. Alkire, A. Canggalari, *J. Electrochem. Soc.*, 136 (1989) 913.
32. C. Deslouis, B. Tyibollet, G. Mengoli, M. M. Musion, *J. Appl. Electrochem.*, 18 (1988) 374.
33. T. Aben, D. Tromans, *J. Electrochem. Soc.*, 142 (1995) 398.
34. A.A. El Warraky, H.A. El Shayeb, and E.M. Sherif, *Anti- Corros. Method. Mater.*, 51 (2004) 52.
35. A.A. El Warraky, H.A. El Shayeb, and E.M. Sherif, *Egypt. J. Chem.*, 47 (2004) 657.
36. A.A. El Warraky, H.A. El Shayeb, and E.M. Sherif, *Egypt. J. Chem.*, 47 (2004) 609.
37. A.E. El Meleigy, M.F. Shehata, G.I. Youssef, Sh.E. Abd El Hamid, A.A. El Warraky, *Ochrona Przed Korozja (Corros. Prot.) nr 10* (2012) 427.
38. G.I. Youssef, M.F. Shehata, A.E. Meleigy, A.A. Warraky, A.M.A. Aziz, *Ochrona Przed Korozja (Corros. Prot.)*, nr 2 (2013) 34.
39. W.J. Van Ooij, *Surf. Technol.*, 6 (1977) 1.
40. H.W. Pickering, P.J. Byrne, *J. Electrochem. Sci.*, 116 (1969) 1492.
41. H.W. Pickering, P.J. Byrne, *J. Electrochem. Sci.*, 118 (1971) 209.

© 2020 The Authors. Published by ESG (www.electrochemsci.org). This article is an open access article distributed under the terms and conditions of the Creative Commons Attribution license (<http://creativecommons.org/licenses/by/4.0/>).